https://doi.org/10.5194/acp-2020-939
Preprint. Discussion started: 12 October 2020

Atmospheric Chemistry and Physics Discussions

Secondary aerosol formation alters CCN activity in the North China Plain

Jiangchuan Tao[1], Ye Kuang[1], Nan Ma[1], Juan Hong[1], Yele Sun[2, 3, 4], Wanyun Xu[5], Yanyan Zhang[1], Yao He[2], Qingwei Luo[1], Linhong Xie[1], Hang Su[6], Yafang Cheng[6]

[1]Institute for Environmental and Climate Research, Jinan University, Guangzhou, Guangdong 511443, China

[2]State Key Laboratory of Atmospheric Boundary Layer Physics and Atmospheric Chemistry, Institute of Atmospheric Physics, Chinese Academy of Sciences, Beijing 100029, China

[3]College of Earth and Planetary Sciences, University of Chinese Academy of Sciences, Beijing 100049, China

[4]Center for Excellence in Regional Atmospheric Environment, Institute of Urban Environment, Chinese Academy of Sciences, Xiamen 361021, China

[5]State Key Laboratory of Severe Weather, Key Laboratory for Atmospheric Chemistry, Institute of Atmospheric Composition, Chinese Academy of Meteorological Sciences, Beijing, 100081, china

[6]Multiphase Chemistry Department, Max Planck Institute for Chemistry, Mainz 55128, Germany

Correspondence to: Jiangchuan Tao (taojch@jnu.edu.cn) and Nan Ma (nan.ma@jnu.edu.cn)

https://doi.org/10.5194/acp-2020-939
Preprint. Discussion started: 12 October 2020

Atmospheric Chemistry and Physics Discussions

Abstract:

The formation of secondary aerosols (SA, including secondary organic and inorganic aerosols, SOA and SIA) is the dominant source of aerosol particles in the North China Plain and has a significant impact on the variations of particle size distribution (PNSD) and hygroscopicity. Previous studies have shown that the mechanism of SA formation can be affected by relative humidity (RH), and thus has different influences on the aerosol hygroscopicity and PNSD under different RH conditions. Based on the measurements of size-resolved particle activation ratio (SPAR), hygroscopicity distribution (GF-PDF), $PM_{2.5}$ chemical composition, PNSD, meteorology and gaseous pollutants in a recent field campaign McFAN (Multiphase chemistry experiment in Fogs and Aerosols in the North China Plain) conducted at Gucheng site from 16th November to 16th December in 2018, the influences of SA formation on CCN activity and CCN number concentration（N_{CCN}) calculation under different RH conditions were studied. Measurements showed that during daytime the SA formation can lead to a significant increase of N_{CCN} and a strong diurnal variation of CCN activity. During periods with minimum RH higher than 50% in daytime (high RH conditions), SA formation significantly contributed to the particle mass/size changes in wide particle size range of 150 nm to 1000 nm, and lead to the increase of N_{CCN} in particle size range of 200 nm to 300 nm while increase of particle mass concentration mainly in particle size larger than 300nm. During periods with minimum RH lower than 30% in daytime (low RH conditions), SA formation mainly contributed to the particle mass/size changes in particle size smaller than 300 nm and so did the increases of both N_{CCN} and particle mass concentration. As a result, upon the same amount of mass increase through SA formation, the increase of N_{CCN} is weaker under high RH conditions while stronger under low RH conditions. Moreover, the diurnal variations of aerosol mixing state (inferred from CCN measurements) due to SA formation was different under different RH conditions, which contributed one of the largest uncertainties in N_{CCN} predictions. By applying aerosol mixing state estimated by number fraction of hygroscopic particles from measurements of particle hygroscopicity or mass fraction of SA from measurements of particle chemical compositions, the N_{CCN} prediction was largely improved with relative deviations smaller than 30%. This study highlights the impact of SA formation on CCN activity and N_{CCN} calculation, which is of great significance for improving parameterization of SA formation in chemical-transport models and CCN predictions in climate models.

https://doi.org/10.5194/acp-2020-939
Preprint. Discussion started: 12 October 2020


Atmospheric Chemistry and Physics Discussions

1. Introduction

CCN activity of aerosol particles has important influence on cloud microphysics and aerosol indirect effect. Formation of secondary aerosol (SA) is an important source of aerosol particles and can provide particles large enough to act as CCN (Wiedensohler et al., 2009; Kerminen et al., 2012; Farmer et al., 2015). In addition, SA formation can affect the size and chemical compositions of existing particles, thus can significantly affect CCN activity of existing particles (Farmer et al., 2015).

SA formation can enlarge particle size by adding secondary mass, and change particle chemical compositions depending on the precursor and mechanism of SA formation (Dal Maso et al., 2005; Kulmala et al., 2007; Zhang et al., 2012; Farmer et al., 2015; Cheng et al., 2016; Kuang et al., 2020b). As particle size and chemical composition (determine aerosol hygroscopicity) are the most dominating factors for CCN activity, the SA formation can generally enhance CCN number concentration (N_{CCN}) and may also change the CCN activity of particles (Wiedensohler et al., 2009; Kerminen et al., 2012; Wu et al., 2015; Farmer et al., 2015; Ma et al., 2016; Zhang et al., 2019 and reference therein). SA formation includes the formation and subsequent growth of new particles (New Particle Formation, NPF), and the growth of existing particles. In general, NPF leads to variation of aerosol particles smaller than 100 nm and thus enhance N_{CCN} at higher supersaturations (SSs>0.2%) (Wiedensohler et al., 2009; Kerminen et al., 2012; Ma et al., 2016; Zhang et al., 2019 and reference therein). Meanwhile, SA formation on existing particles, especially under polluted conditions, can also significantly contribute to the formation of accumulation mode particles and affect CCN at lower SSs (<0.2%) (Wiedensohler et al., 2009; Mei et al., 2013; Yue et al., 2016; Thalman et al., 2017; Duan et al., 2018). Although there are large variations of SSs in different categories of clouds, stratus clouds and fogs, which have strong effects on climate and environment, generally form at SSs lower than 0.2% that only accumulation mode particles can serve as CCN (Ditas et al., 2012; Hammer et al., 2014a, b; Krüger et al., 2014; Shen et al., 2018). In addition, the interactions between aerosol and clouds in stratus clouds and fogs are quite different with those in cumulus clouds which formed under higher SSs and were influenced by Aitken mode particles formed in NPF events (Reuter et al., 2009; Gryspeerdt and Stier, 2012; Fan et al., 2016; Jia et al., 2019 and reference therein). Thus, SA formation on existing accumulation mode particles can have unique influence on climate and environment, highlighting the importance of investigating the influence of SA formation on CCN activity of existing particles.

SA formation affects CCN activity of accumulation mode particles by not only enlarging particle size but also changing particle chemical compositions. In detail, at a specific particle size, CCN activity of particles after SA formation is determined by chemical compositions of particles that

https://doi.org/10.5194/acp-2020-939
Preprint. Discussion started: 12 October 2020


Atmospheric Chemistry and Physics Discussions

has smaller particle size before SA formation and grow to this specific size. Thus, there can be different variations in CCN activity at the same particle size, which is determined by chemical compositions of both the original particles and the growing particles (Wiedensohler et al., 2009 and reference therein). Compared with numerous studies about the impact of NPF on CCN (Gorden et al., 2016; Yu et al., 2020 and reference therein), few studies focus on the influence of SA formation on CCN activity of accumulation mode particles. In general, the formation of SA can transfer hydrophobic particles to hydrophilic particles by adding chemical compounds with lower volatility and higher oxidation state, which usually is more hydrophilic, and thus enhance CCN activity of accumulation mode particles (Mei et al., 2013; Yue et al., 2016). However, CCN activity may also remain unchanged (Wiedensohler et al., 2009) or become weaker in some cases (Thalman et al., 2017; Duan et al., 2018). In SA formation observed in central Amazon forests, Thalman et al. (2017) reported enhanced CCN activity in dry season while constant CCN activity in wet season. In SA formation under polluted conditions in Guangzhou, Duan et al. (2018) found that bulk CCN activity can be enhanced in summer due to the formation of large and inorganic-rich particles, but weakened in winter due to the formation of small and organic-rich particles, and RH seemed to be an important factor in the variations of bulk CCN activity due to different particle formation pathways. Besides the variations of particle chemical composition, the variations of mixing states of aerosol particles in SA formation can also change the CCN activity of aerosol (Su et al., 2010; Rose et al., 2011; Cheng et al., 2012). Due to the fast condensation of accumulation mode particle in SA formation, the turnover of soot particles mixing state from externally mixed to internally mixed mainly contributed to enhancement of CCN activity (Cheng et al., 2012). Thus, it is necessary to conduct more comprehensive study on the influence of SA formation on CCN activity of accumulation mode particles.

On the North China Plain (NCP), there is serious aerosol pollution because of strong emission of primary aerosol and strong SA formation due to abundant gaseous precursors (Zheng et al. ACP, 2015; Liu et al., 2010; Huang et al., 2014; Xu et al., 2019). In the formations of SA on the NCP, both aqueous-phase processes and gas-phase photochemical processes can play an important role, depending on the atmospheric conditions like RH (Hu et al., 2016; Xu et al., 2017; Wang et al., 2019). Recently, observation study on the NCP found that the particle size where SA formation dominated can be different due to different SA formation mechanisms under different RH conditions (Kuang et al., 2020b). Under dry conditions, SA are mainly formed through gas-phase photochemical processing and adding mass to accumulation mode particles. While under high RH conditions or super-saturated conditions, SA can also be formed in aqueous phase through further oxidation of gaseous precursors that contribute to the formation of both accumulation mode particles and coarse mode particles. The

https://doi.org/10.5194/acp-2020-939
Preprint. Discussion started: 12 October 2020


Atmospheric Chemistry and Physics Discussions

difference of particle size where SA formation taking place and the different chemical compositions of SA can result in different variation of CCN activity. Thus, it is essential to study the influence of SA formation on CCN activity of accumulation mode particles under different RH conditions on the NCP.

2. Method:

2.1. Measurements

2.1.1. Site

Under the framework of McFAN (Multiphase chemistry experiment in Fogs and Aerosols in the North China Plain) (Li et al., submitted), from 16th November to 16th December 2018, physical and chemical properties of ambient aerosol particles as well as meteorological parameters were continuously measured at the Gucheng site in Dingxing county, Hebei province, China. This site is an Ecological and Agricultural Meteorology Station (39°09'N, 115°44'E) of the Chinese Academy of Meteorological Sciences, which is located between Beijing (~ 100km) and Baoding (~40km), two large cities on the North China Plain and surrounded by farmlands and small towns. Measurements at this site can well represent the background conditions of atmospheric pollution on the NCP. All the instruments of aerosol measurement were placed in a container with the temperature maintained at 24 °C, and the conventional trace gas instruments including CO were housed in an air-conditioned room on a two-story building located in the south of the container.

2.1.2 Instrumentation

In this study, ambient aerosol was sampled by an inlet system consisting of a PM10 inlet (Rupprecht & Patashnick Co., Inc., Thermo, 16.67 L/min), dried to relative humidity below 30% by a Nafion dryer and directed to each instrument using an isokinetic flow splitter.

A DMA-CCNC system measured CCN activity of particles at five supersaturations (SSs) of 0.07%, 0.1%, 0.2%, 0.4% and 0.8%, and the running time was 20 min for 0.07% and 10 min for the other SSs. The corrected SSs levels were 0.05%, 0.07%, 0.2%, 0.4% and 0.8%. This system consisted of a differential mobility analyzer (DMA model 3081; TSI, Inc, MN USA), a condensation particle counter (CPC model 3772; TSI, Inc., MN USA) and a continuous-flow CCN counter (model CCN200, Droplet Measurement Technologies, USA; Roberts and Nenes, 2005). The system was operated in a size-scanning mode over the particle size range from 9 to 300 nm. Size-resolved Particle Activation Ratio (SPAR) can be obtained by combining the measurements of CPC and CCNC at different particle

https://doi.org/10.5194/acp-2020-939
Preprint. Discussion started: 12 October 2020


Atmospheric Chemistry and Physics Discussions

size. The sample and sheath flow rate of the DMA were set to 1 lpm and 5 lpm, respectively, hence the resultant measured particle diameter ranged from 9 nm to 500 nm. Because of the low number concentration of particles above 300 nm could lead to large uncertainty in CCNC counting, the measurements for particles larger than 300 nm are excluded. There are 12 size distribution scans during a complete 1-hour cycle, with four scans for first SS and two scans for each of the rest four SSs. Only the last scan for each SS is used as the CCNC needs time for SS stabilization. The SS of CCNC were calibrated with monodisperse ammonium sulphate particles (Rose et al., 2008) both before and after the campaign. And the flowrates were checked regularly (once every several days) during the campaign, as the flows (sample flow and sheath flow) of the instrument can affect both the counting of droplets and the supersaturation formed in the column. A modified algorithm based on Hagen and Alofs (1983) and Deng et al. (2011, 2013) was used to correct the influence of multiple-charge particles on SPAR. Details about the system are described in Ma et al. (2016).

Non-refractory particulate matter (NR-PM) including organics, SO_4^{2-}, NO_3^-, NH_4^+ and Cl^- with dry aerodynamic diameters below 2.5μm was measured by an Aerodyne Time-of-Flight Aerosol Chemical Speciation Monitor (ToF-ACSM hereafter) equipped with a $PM_{2.5}$ aerodynamic lens (Williams et al., 2010) and a capture vaporizer (Xu et al., 2017; Hu et al., 2017) at 2-minute time resolution. The ToF-ACSM data were analyzed with the standard data analysis software (Tofware v2.5.13; https://sites.google.com/site/ariacsm/, last access: 21 January 2020). The organic mass spectra from *m/z* 12 to 214 were analyzed with an Igor Pro based positive matrix factorization (PMF) evaluation tool (v3.04) and then evaluated following the procedures described in Zhang et al. (2011). The chosen five-factor solution includes four primary factors i.e. hydrocarbon-like OA (HOA), cooking OA (COA), biomass burning OA (BBOA), and coal combustion OA (CCOA), and one secondary factor, i.e. oxygenated OA (OOA). More detailed descriptions on the ACSM measurements and data analysis can be found in Kuang et al. (2020a) and Sun et al. (2020).

A Humidified Tandem differential mobility analyzer (HTDMA, Tan et al., 2013) measured the size-resolved aerosol growth factor (GF) under RH of 90 %. The sampled particles were subsequently charged by a neutralizer (Kr85, TSI Inc.) and size selected by a DMA (DMA1, model 3081L, TSI Inc.). A Nafion humidifier (model PD-70T-24ss, Perma Pure Inc., USA) was used to humidified the monodisperse particles with a specific diameter (D_0) under a fixed RH of (90 ± 0.44) % and then the number size distribution of the humidified particles (Dd) was measured by another DMA (DMA2, model 3081L, TSI Inc.) and a condensation particle counter (CPC, model 3772, TSI Inc.). Thus, GF of the particles can be calculated as:

https://doi.org/10.5194/acp-2020-939
Preprint. Discussion started: 12 October 2020

Atmospheric Chemistry and Physics Discussions

$$GF=\frac{D_d}{D_0} \quad (1)$$

During the campaign, five dry mobility diameters (60, 100, 150, and 200 nm) were selected for the HTDMA measurements. A full scan takes about 1 hour in order to cover the six sizes. Regular calibration by using standard polystyrene latex spheres and ammonium sulfate were performed to ensure the instrument functioned normally. The tandem differential mobility analyzer (TDMA) inversion algorithm (Gysel et al., 2009) was applied to calculate the Probability Density Function of GF (GF-PDF). More details about this system can be referred to Cai et al. (2018) and Hong et al. (2018).

A commercial instrument from Thermo Electronics (Model 48C) was used to measure CO concentration. Besides monthly multipoint calibrations and weekly zero-span check, additional 6-hourly zero checks were also performed for the CO instrument. Particle number size distributions (PNSDs) were measured by combining the measurements of a scanning mobility particle sizer (SMPS, TSI model 3080) and an aerodynamic particle sizer (APS, TSI Inc., Model 3321), that measured particle mobility diameter size distributions in the range of 12 nm to 760 nm and particle aerodynamic diameter size distribution in the range of 700 nm to 10 μm, respectively.

2.2. Data processing

2.2.1. Aerosol hygroscopicity and cloud activation: κ-Kohler theory

The ability of particles to act as CCN and its dependence on particle size and particle chemical composition on CCN activity can be described by the Köhler theory (Köhler, 1936). A hygroscopic parameter κ is calculated based on the κ-Köhler theory (Petters and Kreidenweis. 2007) to evaluate the influence of particles chemical compositions:

$$\kappa=\left(\frac{D_{wet}^3-D_d^3}{D_d^3}\right)\left[\frac{1}{S}\exp\left(\frac{4\sigma_{s/a}M_w}{RT\rho_w D_{wet}}\right)-1\right] \quad (1)$$

where S represents the saturation ratio, ρ_w is the density of water, M_w is the molecular weight of water, $\sigma_{s/a}$ is the surface tension of the solution/air interface, R is the universal gas constant, T is the temperature, D_d is the diameter of dry particle and D_{wet} is the diameter of the humidified particle. In this study, $\sigma_{s/a}$ is assumed to be the surface tension of the pure water/air interface. Based on the κ-Kohler theory, the surface equilibrium water vapor saturation ratio of particles with a specific κ at different wet particle size can be calculated, and the maximum value of surface equilibrium saturation ratio (which is generally supersaturated) is defined as the critical SS for CCN activation. As a result,

https://doi.org/10.5194/acp-2020-939
Preprint. Discussion started: 12 October 2020


Atmospheric Chemistry and Physics Discussions

the variation of the critical diameter for particles with different hygroscopicity (or GF at a specific RH) at different SSs can be determined.

2.2.2. Aerosol growth factor and its probability density function

In practice, the growth factor probability density function (GF-PDF) was fitted from the measured GF distribution using a TDMAinv algorithm (Gysel et al., 2009). After obtaining the GF-PDF, the ensemble average GF (HGF?) and corresponding critical diameter under a certain SS (Da_HGF) can be calculated. Furthermore, the number fractions and the HGF of hygroscopic particles (κ >0.1 and GF(90%, 200nm)>1.22) were calculated:

$$NF_{hygro} = \int_{1.2}^{\infty} PDF(GF) \times dGF \quad (2)$$

$$GF_{hygro} = \int_{1.2}^{\infty} GF \times PDF(GF) \times dGF \quad (3)$$

Based on the κ-Kohler theory, the hygroscopicity parameter κ and critical diameter under a certain SS (Da_hygro) can be calculated.

2.2.3 Calculations of aerosol hygroscopicity from aerosol chemical-composition measurements

For the calculation of aerosol hygroscopicity parameter κ based on measured chemical composition data (κ_{chem}), detailed information on the chemical species are needed. The ACSM can only provide bulk mass concentrations of SO_4^{2-}, NO_3^-, NH_4^+, Cl^- ions and organic components, which cannot be used to calculate the mass fraction of particle chemical composition at a specific particle size. However, in the North China Plain, the particle mass concentration of accumulation mode particles are the dominate contributors of the bulk particle mass concentration (Liu et al., 2014; Xu et al., 2015; Hu et al., 2017) and thus the variation of bulk mass fraction of particle chemical composition can be used as a proxy of the variation of mass fraction of accumulation mode particles. For the inorganic ions, a simplified ion pairing scheme was used to convert ion mass concentrations to mass concentrations of corresponding inorganic salts (Gysel et al., 2007; Wu et al., 2016). Thus, mass concentrations of SO_4^{2-}, NO_3^-, NH_4^+ and Cl^- are specified into ammonium sulfate (AS), ammonium nitrate (AN), ammonium chloride (AC) and ammonium bisulfate (ABS), with the κ values of these salts specified according to Liu et al. (2014). For a given internal mixture of different aerosol chemical species, the Zdanovskii–Stokes–Robinson (ZSR) mixing rule can be used for predicting the overall κ_{chem} on the basis of volume fractions of different chemical species (ε_i) (Petters and Kreidenweis, 2007):

$$\kappa_{chem} = \sum_i \kappa_i \cdot \varepsilon_i \quad (4)$$

https://doi.org/10.5194/acp-2020-939
Preprint. Discussion started: 12 October 2020


Atmospheric Chemistry and Physics Discussions

where κ_i and ε_i represent the hygroscopicity parameter κ and volume fraction of chemical component *i* in the mixture. Based on Eq.2, κ_{chem} can be calculated as follows:

$$\kappa_{chem}=\kappa_{AS}\varepsilon_{AS}+\kappa_{AN}\varepsilon_{AN}+\kappa_{ABS}\varepsilon_{ABS}+\kappa_{AC}\varepsilon_{AC}+\kappa_{BC}\varepsilon_{BC}+\kappa_{Org}\varepsilon_{Org} \quad (5)$$

where κ_{org} and ε_{org} represent κ and volume fraction of total organics. There are large variations of κ_{org} in former studies and a linear relationship reported in the same campaign between κ_{org} and organic aerosol oxidation state (f44 in specific, Kuang et al., 2020a) was used to calculate κ_{org} in this study:

$$\kappa_{OA}=1.04\times f44-0.02 \quad (6)$$

κ_{BC} is assumed to be zero as black carbon is hydrophilic.

2.2.4. Fitting parameterization scheme of SPAR

In general, the variations of CCN activity for particle population can be attributed to variations of the number fraction or the hygroscopicity for hygroscopic particles, which can be indicated by fitting parameters of SPAR curves parameterization. SPAR curves are generally parameterized with a sigmoidal function with three parameters. This parameterization assumes aerosols to be an external mixture of apparently hygroscopic particles that can act as CCN and hydrophobic particles that cannot be measured by CCNC (Rose et al., 2010). For SPAR (*R*a(*D*p)) at a specific SS, the formula is as follows (Rose et al., 2008):

$$\mathrm{Ra(Dp)}=\frac{\mathrm{MAF}}{2}\left(1+\mathrm{erf}\left(\frac{D_p-D_a}{\sqrt{2}\sigma}\right)\right) \quad (7)$$

where erf is the error function. MAF is an asymptote of the measured SPAR curve at large particle sizes and can represents the number fraction of CCNs to total particles at particle size around Da. D_a is the midpoint activation diameter and is associated with the hygroscopicity of CCNs. σ is the standard deviation of the cumulative Gaussian distribution function and indicates the heterogeneity of CCN hygroscopicity. Although the influence of nearly hydrophobic particles (κ<0.1) on SPAR cannot be considered in this parameterization scheme, deviation can only be found significant under higher SSs (Tao et al., 2020) and need not to be considered under the low SSs discussed in this study.

https://doi.org/10.5194/acp-2020-939
Preprint. Discussion started: 12 October 2020


Atmospheric Chemistry and Physics Discussions

3. Results

3.1. Overview of the measurements

The timeseries of meteorological parameters, particle CCN activity, N_{CCN} at SS of 0.05% and mass concentration of Non-refractory particulate matter of $PM_{2.5}$ (NR-$PM_{2.5}$), $PM_{2.5}$ SA and $PM_{2.5}$ PA are shown in Fig. 1. Strong diurnal variations, especially for meteorological parameters and CCN activity, can be found. During the whole period, the wind speed is generally lower than 4m/s and in favor of accumulation of aerosol particles and formation of SA on existing particles. However, there were systematic difference of RH, N_{CCN}, mass concentration of $PM_{2.5}$ SA and NR-$PM_{2.5}$ before and after 4th Dec, and thus the whole campaign can be divided into two parts with different RH conditions and SA pollution conditions: higher RH and stronger SA pollution before 4th Dec, and lower RH and lighter SA pollution after 4th Dec. In following discussions, high RH conditions correspond to the periods before 4th Dec. whose daily maximum and minimum RH are generally higher than 75% and 50%, respectively, especially from 25th Nov to 27th Nov (Event 1) and from 30th Nov to 2nd Dec (Event 2) with fog events during these days (blue shaded areas), and low RH conditions correspond to the periods after 4th Dec whose daily maximum and minimum RH are generally lower than 70% and 30%, especially from 9th Dec to 11th Dec (Event 3). As reported in Kuang et al. (2020b), these high RH conditions promote SA formation in aerosol liquid water content and lead to a persistent increase of N_{CCN}, mass concentration of NR-$PM_{2.5}$ and especially mass concentration of $PM_{2.5}$ SA during event 1 and 2. Atmospheric RH after 4th Dec are generally lower, with daily maximum lower than 70% and the dominating SA formation were in gas-phase, that generate much less SA than aqueous-phase formation (Kuang et al., 2020b). Thus, the persistent increases of N_{CCN} and $PM_{2.5}$ from 7th Dec to 11th Dec (Event 3) are much weaker than those in events 1 and 2. Due to the different SA contributions to total particles, CCN activity before 4th Dec are generally stronger than that after 4th Dec. The ratios between N_{CCN} and mass concentration of $PM_{2.5}$ SA or NR-$PM_{2.5}$, were lower after 4th Dec than those before 4th Dec and demonstrated decreasing trends especially in SA formation events under high RH conditions. The response of CCN activity and N_{CCN} to the different SA formation mechanism will be discussed comprehensively in the following parts.

3.2. The influence of different secondary aerosol formation on the diurnal variation of CCN activity

The diurnal averages of aerosol CCN activity at SS of 0.05%, GF-PDF for 200nm particle and mass fraction of particle chemical compositions during the three events are shown in Fig. 2, respectively. There were simultaneously increases of particle CCN activity, aerosol hygroscopicity

https://doi.org/10.5194/acp-2020-939
Preprint. Discussion started: 12 October 2020


Atmospheric Chemistry and Physics Discussions

293 and mass fraction of SA during daytime for all the three events, suggesting that the enhancement of
294 particle CCN activity was mainly due to the increase of hygroscopic particles in SA formation. In
295 general, there were stronger particle CCN activity, higher aerosol hygroscopicity and higher mass
296 fraction of SA in events 1 and 2 than those in event 3. In events 1 and 2, it can be found that SPAR
297 values are generally higher than 0.5 at 200nm and can reach the maximum of 1 at noon at 300nm. A
298 hygroscopic mode with GF>1.4 can be found throughout the day and dominates aerosol hygroscopicity
299 during the daytime. Mass fraction of SA were generally higher than 70% and reach the maximum of
300 0.8 at noon. While in event 3, SPAR at 200nm is lower than 0.4 at night and the maximum of SPAR
301 at 300nm was lower than 0.9. A hydrophobic mode with GF<1.1 dominates particle hygroscopicity,
302 and the mass fraction of SA was lower than 60% and 30% at noon and at night, respectively. However,
303 the increase of SA mass fraction at noon in event 3 was stronger than those in events 1 and 2 and a
304 stronger enhancement of particle CCN activity at noon in event 3 can be speculated.

305 In Fig. 3, detailed comparison of particle CCN activity during events of N_{CCN} enhancements
306 under different RH conditions are shown as the variations of SPAR curves. Particle CCN activity in
307 event 1 and 2 were combined due to their similar diurnal variation shown in Fig. 2. Besides SPAR
308 curves (Fig. 3(a)), corresponding fitting parameter of SPAR curve including Da and MAF were also
309 shown (Fig. 3(b) and (c)), as enhanced CCN activity for particle population can be attribute to increase
310 of the number fraction for hygroscopic particles (increase of MAF) or enhancement of hygroscopicity
311 for hygroscopic particles (decrease of Da). Same as that demonstrated in Fig. 2, particle CCN activity
312 were generally stronger in high RH events (event 1 and 2) than that in low RH events (event 3).
313 However, the enhancement of particle CCN activity was stronger in low RH events, probably due to
314 both the stronger increase of mass fraction of SA and higher mass fraction of PA at nighttime as shown
315 in Fig. 2. Furthermore, in high RH events, there were enhancements of CCN activity from 150nm to
316 300nm during daytime, which was characterized as the increase of MAF and decrease of Da during
317 daytime and mainly resulted from the increase of number fraction and hygroscopicity of CCN-active
318 particle. While in low RH events, the enhancement of CCN activity at noon were just at particle size
319 larger than 200nm. This can be attribute to the increases of Da and MAF, indicating increasing number
320 fraction but weakening hygroscopicity of hygroscopic particles, respectively. In summary, in high RH
321 events, the enhancement of CCN activity was lighter but at broader particle size range than that in
322 event 3. As reported by Kuang et al. (2020b), the SA formation in event 1 and 2 under high RH
323 conditions occurred in both gaseous phase and aqueous phase, and formed SA mainly at larger particle
324 size up to 1um, while SA formation in event 3 under low RH conditions dominantly occurred in gas-
325 phase and formed SA at particle size smaller than 300nm. At particle size smaller than 200nm where

https://doi.org/10.5194/acp-2020-939
Preprint. Discussion started: 12 October 2020


Atmospheric Chemistry and Physics Discussions

326 SA can form at both low and high RH conditions, there was increase of CCN activity at high RH
327 conditions while unchanged CCN activity at low RH conditions. Under high RH conditions, the
328 enhanced CCN activity can be attributed to the large contribution of secondary inorganic compounds
329 to particle secondary compounds in SA formation, which can be higher than 70%. Under low RH
330 conditions, the almost unchanged CCN activity at particle size of about 200nm may be due to
331 unchanged particle hygroscopicity before and after SA formation, as nearly half of secondary
332 compounds to be secondary organic compounds in SA formation under low RH conditions and SOA
333 has much lower hygroscopicity than SIA.

334 As there were different influences of SA formation on both CCN activity and PNSD under
335 different RH conditions, different variation of N_{CCN} due to the SA formation can be expected. In Fig.
336 4, the diurnal variation of $PM_{2.5}$, particle volume concentration (Vconc), N_{CCN} normalized by CO and
337 the ratio between N_{CCN} and $PM_{2.5}$ during high and low RH events were analyzed. The variation of
338 Vconc in different particle size range can be used to speculate the variation of NR-$PM_{2.5}$ of different
339 particle size range considering the relatively smaller variations of particle density. By dividing the
340 concentration of CO, diurnal variation due to PBL can be partially compensated and thus a more direct
341 quantification of the influence of SA formation on the diurnal variation can be obtained. The variations
342 of the ratio between N_{CCN} (in different particle size range) and the mass concentration of $PM_{2.5}$ SA
343 (referred as to N_{CCN}/SA) or NR-$PM_{2.5}$ (referred as to N_{CCN}/NR) can be used to evaluate the response
344 of N_{CCN} to SA formation.

345 During high RH events from 8:00 to 14:00, normalized N_{CCN} increased by about 50% and a
346 similar increase of $PM_{2.5}$ SA mass concentration can be also found (Fig. 4(a1)). As the decrease of
347 mass concentration of $PM_{2.5}$ PA was much smaller than the increase of $PM_{2.5}$ SA mass concentration,
348 the increase of NR-$PM_{2.5}$ mass concentration to can be expected to be similar to the increase of $PM_{2.5}$
349 SA mass concentration. As reported by Kuang et al. (2020b), SA during daytime were mainly formed
350 at larger particle sizes characterized, as there were increase of Vconc in particle size range of 400nm
351 to 1um. In detail, there were significant increases of particle number concentration (Nconc) in particle
352 size range of 150nm to 1000 nm (Fig. S1(a1)). Because at larger particle size the increase of Nconc
353 lead to stronger increase of Vconc, there was simultaneous but much weaker increases of Vconc in
354 particle size range of 150 nm to 300nm compared with increases of those in particle size of larger than
355 300nm (Fig. 4(b1)), suggesting that $PM_{2.5}$ SA were mainly increased in particle size of larger than
356 300nm. In addition, because of the SA formation enhanced hygroscopicity and number fraction of
357 CCN-active particles in particle size range of 150nm to 300nm, simultaneous enhancements of CCN
358 activity can be found throughout the measured particle size range of 180nm to 300nm (Fig. S1(b1)).

https://doi.org/10.5194/acp-2020-939
Preprint. Discussion started: 12 October 2020


Atmospheric Chemistry and Physics Discussions

By combining the enhancements of Nconc and CCN activity in measured particle size ranges, there were increases of N_{CCN} from 200 nm to 500nm (Fig. 4(c1)). Compared with the strongest increases of Vconc with particle size larger than 300nm, the increase of N_{CCN} was strongest for particle size range of 200nm to 300nm, suggesting that particle larger than 300nm were generally CCN-active before SA formation and thus the growth of these particles due to SA formation lead to increase of volume (thus mass) rather than N_{CCN}. As a result, N_{CCN} (>300nm)/SA, N_{CCN} (<300nm)/SA, N_{CCN} (>300nm)/NR and N_{CCN} (<300nm)/NR all decreased continuously during the SA formation (Fig. 4(d1)), and N_{CCN} /NR became smaller due to the SA formation, suggesting that weakening enhancement of N_{CCN} in SA formation under high RH condition as SA formation mainly adding mass to CCN-active particles before SA formation.

During low RH events, weaker increases of both N_{CCN} and $PM_{2.5}$ SA mass concentration can be found from 8:00 to 14:00. During the same time, PA mass decreased by 50% and the variation of NR mass was small. Under low RH condition, SA formation mainly contributed mass enhancements for smaller particle size as there were enhances of Vconc at particle size range of 150nm to 300nm rather than larger than 300nm (Kuang et al., 2020b). In detail, there were increase of Vconc in the range of 150nm to 300nm (Fig. 4(b2)) as there was increase of Nconc only in the range of smaller than 300nm (Fig. S1(a2)), suggesting that $PM_{2.5}$ SA were mainly increased in particle size of smaller than 300nm. As shown in Fig. 4, there was SA formation caused enhancement of CCN activity only in particle size of 200nm to 300nm and no variation CCN activity only in particle size of 180nm to 200nm (Fig. S1(b2)), mainly due to the SA formation enhanced number fraction of CCN-active particles in particle size of 200 to 300nm. Again, by combining the variation of Nconc and CCN activity at measured particle size ranges, there was only significant increase of N_{CCN} in particle size of 200 nm to 300nm (Fig. 4(c2)). As a result, although N_{CCN} (>300nm)/SA decreased as that under high RH conditions, N_{CCN} (<300nm)/SA and N_{CCN} (>300nm)/NR generally stay constant and N_{CCN} (<300nm)/NR even increased during SA formation in daytime (Fig. 4(d2)). And the ratio between bulk N_{CCN} and mass concentration of NR-$PM_{2.5}$ became larger due to the SA formation, suggesting that stronger enhancement of N_{CCN} in SA formation under low RH condition as SA formation mainly adding mass to CCN-inactive particles before SA formation that turned into CCN-active particles after SA formation.

As shown in Fig. 1, RH were generally higher before 4th Dec and lower after 4th Dec, and the average diurnal variations of variables mentioned in Fig. 4 were also presented in Fig. S2. Compared with the average diurnal variations during the events with significant N_{CCN} enhancement, the average diurnal variations during the high and low RH periods were similar with higher levels of particle mass

https://doi.org/10.5194/acp-2020-939
Preprint. Discussion started: 12 October 2020


Atmospheric Chemistry and Physics Discussions

concentration but weaker enhancement of SA and N_{CCN}, indicating a similar but weaker impact of SA formation on CCN activity due to the interference of other aerosol processes.

In summary, during the campaign in this study, two kinds of SA formation events were observed under different RH conditions with different variations of PM and N_{CCN}. In detail, under high RH conditions, there were strong SA formation and N_{CCN} enhancements, with strong hygroscopicity particles and SIA to dominate. Meanwhile, under low RH conditions, there were moderate SA formation and N_{CCN} enhancements, with moderate hygroscopicity particles and higher SOA contribution. However, as the ratio between N_{CCN} and NR-$PM_{2.5}$ became higher under low RH conditions but lower under high RH conditions, respectively, the increase of N_{CCN} became stronger under low RH conditions while lower under high RH conditions if there formed a same amount of particle mass. This was because the formation of SA under low RH conditions was more concentrated in particle size range of smaller than 300nm and adding more mass to CCN-inactive particles before SA formation that turned into CCN-active particles after SA formation. In addition, strong and different diurnal variations of CCN activity of particles due to the strong and different SA formations were also observed and their effects on N_{CCN} calculation need to be further discussed.

3.3. The influence of diurnal variation of CCN activity on N_{CCN} prediction

In former sections, it was found that there were different variations of PNSD and CCN activity in SA formations under different RH conditions, that resulted in different variation of N_{CCN}. Meanwhile, as the measurement of PNSD was generally more simple and common than measurement of N_{CCN}, it is widely applied for the calculation of N_{CCN} based on real-time PNSD and parameterized CCN activity, and thus it is important to specify the contribution of PNSD and CCN activity on N_{CCN} calculation in SA formations under different RH conditions.

In this study, PNSD dominated the N_{CCN} calculation as generally found in former studies (Dusek et al., 2006), but the variation of CCN activity can also contributed significantly to the deviation of N_{CCN} calculation during SA formation. As shown in former discussions, CCN activity (indicated by SPAR) during this campaign can be generally characterized by significant but different diurnal variations under different RH conditions. The influence of SPAR variations on the deviation of N_{CCN} calculated based on campaign average of CCN activity (N_{CCN_cal}) from measured N_{CCN} (N_{CCN_meas}) are analyzed before and after 4th Dec, as shown in Fig. 5. In detail, as the variations of SPAR was determined by the variation of Da and MAF, which indicated the variations of hygroscopicity and number fraction of hygroscopic particles, the influence of the variation of MAF

https://doi.org/10.5194/acp-2020-939
Preprint. Discussion started: 12 October 2020


Atmospheric Chemistry and Physics Discussions

and Da on N_{CCN_cal} also needs to be discussed. In specific, N_{CCN} calculated based on the real-time PNSD and the estimated SPAR from Eq. 7 based the averaged MAF (or Da) and the real-time Da (or MAF), which referred as to N_{CCN_AvgMAF} (or N_{CCN_avgDa}), were compared with the measured N_{CCN} to investigate the influence of MAF (or Da) variations on N_{CCN}. During daytime before 4th Dec, there can be up to 20% underestimation of N_{CCN_cal} without considering SPAR variation due to the enhancement of CCN activity. In detail, as there were similar deviations of both N_{CCN_AvgMAF} and N_{CCN_avgDa} from N_{CCN_meas}, both the MAF variations and Da variations contributed to the N_{CCN_cal} underestimation under high RH conditions. After 4th Dec, there can be 10% overestimation and 10% underestimation of $N_{CCN\_AvgSPAR}$ beyond and during SA formations, respectively, and there were similar difference between N_{CCN_AvgMAF} and N_{CCN_meas}, which means MAF variations mainly contributed to these differences between N_{CCN_cal} and N_{CCN_meas}, because of significant enhancement of number fraction of CCN-active particles due to SA formations. In summary, there can be significant difference between N_{CCN_cal} and N_{CCN_meas} during daytime due to SA formations, which mainly resulted from the variation of MAF and varied under different RH conditions. Thus, the consideration of the variation of MAF was needed for accurate N_{CCN} calculation.

As CCN-active particles were generally considered to be hygroscopic particles or SA particles (both SIA and SOA), Number Fraction of hygroscopic particles (NF_hygro) measured by HTDMA and Mass Fraction of SA particles (MF_SA) measured by ACSM were used to estimate the variation of MAF and improve the calculation of N_{CCN} combining with PNSD measurement.

Based on the bulk hygroscopicity derived from particle chemical compositions measurements (κ_chem), a critical diameter can be calculated based on κ-Kohler theory and then N_{CCN} can be predicted by combining measured PNSD and the critical diameter (N_{CCN_Chem}). In Fig. 6(a), it can be found that N_{CCN_meas} were strongly underestimated by N_{CCN_Chem}, especially when N_{CCN_meas} were low to about 10^2 #/cm^3. Similar underestimation of calculated N_{CCN} can be found in few studies which observed high fraction of organics (Chang et al., 2010; Kawana et al., 2015). This deviation between N_{CCN_meas} and N_{CCN_Chem} may result from the hypothesis of internally mixing state and the difference of particle hygroscopicity derived by measurement of particle chemical compositions and particle CCN activity. In Fig. 6(b), the correlation between mass fraction of SA (MF_SA) and MAF, and the application of MF_SA on N_{CCN} calculation were shown. Besides a small degree of underestimation, MF_SA strongly correlated with MAF in general (Fig. 6(b)), suggesting that externally mixed SA dominated CCN-active particles. Thus, real-time MAF can be estimated by MF_SA, and the real-time SPAR can be calculated from Eq. 7 based on the real-time estimated MAF, the campaign average of Da and σ (the standard deviation). By introducing SPAR with Da and MAF derived by hygroscopicity

https://doi.org/10.5194/acp-2020-939
Preprint. Discussion started: 12 October 2020


Atmospheric Chemistry and Physics Discussions

and MF of SA into N_{CCN} calculation, the underestimation and the correlation between N_{CCN_cal} and N_{CCN_meas} can be significantly improved (Fig. 6(c)).

Based on the bulk hygroscopicity derived from GF measurement (kappa_HGF) at 200nm, a critical diameter can be calculated based on κ-Kohler theory and then N_{CCN} can be predicted by combining measured PNSD and the critical diameter (N_{CCN_HGF}). In Fig. 7(a), it can be found that N_{CCN_meas} were strongly underestimated by N_{CCN_HGF} by more than 30%. This deviation between N_{CCN_meas} and N_{CCN_HGF} may result from the hypothesis of internally mixing state and the difference of particle hygroscopicity derived by GF and particle CCN activity measured under different water vapor saturated conditions. In Fig. 7(b), the correlation between NF_hygro and MAF, and the application of NF_hygro on N_{CCN} calculation were shown. There was also positive correlation between NF_hygro and MAF, although weaker than MF_SA. The same as , the real-time MAF can be estimated by NF_hygro, and the real-time SPAR can be calculated from Eq. 7 based on the real-time estimated MAF, the campaign average of Da and σ (the standard deviation) (the standard deviation). By introducing SPAR calculated with Da and MAF derived by hygroscopicity and NF of hygroscopic particles into N_{CCN} calculation, the underestimation and the correlation between N_{CCN_cal} and N_{CCN_meas} can be significantly improved (Fig. 7(c)).

In summary, as there was strong diurnal variation of MAF, which were also varied under different RH conditions, it is necessary to consider the variation of MAF in N_{CCN} calculation. As the fraction of CCN-active particles were generally hygroscopic and composed of secondary compounds, there were good correlation between MAF, MF_SA and NF_hygro. Thus, by applying MAF estimated by MF_SA or NF_hygro into the derive SPAR curve, the calculation of N_{CCN} can be significantly improved.

https://doi.org/10.5194/acp-2020-939
Preprint. Discussion started: 12 October 2020


Atmospheric Chemistry and Physics Discussions

4. Conclusions

SA formation drives the development of haze pollution on the NCP and can result in significant variations of PNSD and aerosol hygroscopicity. Studies on the NCP have shown that the mechanism of SA formation can be affected by relative humidity (RH), and thus has different influences on the aerosol hygroscopicity and PNSD under different RH conditions. The difference of particle size where SA formation taking place and the different chemical compositions of SA can result in different variation of CCN activity. Thus, it is essential to study the influence of SA formation on CCN activity of existing accumulation mode particles under different RH conditions on the NCP. And as it is widely applied for the calculation of N_{CCN} based on real-time PNSD and parameterized CCN activity, the influence of varied CCN activity of SA particles on N_{CCN} calculation need to be discussed in detail.

Based on the measurements of CCN-activity, particle hygroscopicity, particle chemical composition, PNSD, conventional meteorology and gaseous pollutants in Gucheng campaign in winter in 2018, the influences of SA formation on CCN activity and N_{CCN} calculation under different RH conditions were studied. Two kinds of SA formation events were observed under different RH conditions with different variations of PM and N_{CCN} during the campaign in this study. Under high RH conditions, which corresponds to the periods with minimum RH higher than 40% in daytime, there were strong SA formation and N_{CCN} enhancements with strong hygroscopicity particles and SIA to contribute more than 70% of the secondary compounds. While under low RH conditions, which corresponds to the periods with minimum RH lower than 30% in daytime, there were moderate SA formation and N_{CCN} enhancements with moderate hygroscopicity particles and SOA to contribute nearly half of the secondary compounds. However, the increase of N_{CCN} if there formed a same amount of particle mass became stronger under low RH conditions but weaker under high RH conditions. This was because the formation of SA under low RH conditions was more concentrated in particle size range of smaller than 300nm and adding more mass to CCN-inactive particles before SA formation that turned into CCN-active particles after SA formation.

In addition, strong and different diurnal variations of CCN activity of particles due to the strong and different SA formations were also observed, and there can be significant underestimation of N_{CCN} if the variations of aerosol mixing state were not considered. As the fraction of CCN-active particles were generally hygroscopic and composed of secondary compounds, there were good correlation among aerosol mixing state inferred from measurements of CCN activity, particle hygroscopicity and particle chemical compositions. Thus, the calculation of NCCN can be significantly improved by applying this aerosol mixing state estimated from measurements of particle hygroscopicity or particle chemical compositions.

https://doi.org/10.5194/acp-2020-939
Preprint. Discussion started: 12 October 2020


Atmospheric Chemistry and Physics Discussions

513 This study can further the understanding of the impact of SA formation on CCN activity and
514 N_{CCN} calculation, specifically for SA formations on existing particles which can strongly affect cloud
515 microphysics properties in stratus clouds and fogs. The investigation of the influence of SA formation
516 on CCN activity of existing particles in this study is important for improving parameterization of SA
517 formation in chemical-transport models and CCN predictions in climate models.

518

519 **Supporting Information**

520 The supporting information is available in a separate file.

521 **Data availability.**

522 The data used in this study are available from the corresponding author upon request
523 (taojch@jnu.edu.cn and nan.ma@ jnu.edu.cn)

524 **Author contributions.**

525 JT, YK and NM designed this research. JT performed the data analysis and wrote the manuscript. YC,
526 HS, NM, YK, JT, and JH planned this campaign. JT and YZ conducted the CCN measurements. YS
527 and YH conducted the ACSM measurements and the ACSM PMF analysis. JH and QL conducted the
528 HTDMA measurements. LX and YZ conducted the particle number size distribution measurements.
529 WX conducted the measurements of CO and meteorological parameters. YC, HS, YS, YK and NM
530 contributed to the revisions of this manuscript and all other coauthors have contributed to this paper in
531 different ways.

532 **Acknowledgement**

533 We acknowledge the National Key Research and Development Program of China (grant no.
534 2017YFC0210104) and the National Natural Science Foundation of China (grant no. 91644218 and
535 41805110).

536 **Conflicts of interest**

537 There are no conflicts to declare.

538

539

https://doi.org/10.5194/acp-2020-939
Preprint. Discussion started: 12 October 2020

Reference:

Cai, M., Tan, H., Chan, C. K., Qin, Y., Xu, H., Li, F., Schurman, M. I., Liu, L. and Zhao, J.: The size-resolved cloud condensation nuclei (CCN) activity and its prediction based on aerosol hygroscopicity and composition in the Pearl Delta River (PRD) region during wintertime 2014, Atmos. Chem. Phys., 18(22), 16419–16437, doi:10.5194/acp-18-16419-2018, 2018.

Dal Maso, M., Kulmala, M., Riipinen, I., Wagner, R., Hussein, T., Aalto, P. P. and Lehtinen, K. E. J.: Formation and growth of fresh atmospheric aerosols: eight years of aerosol size distribution data from SMEAR II, Hyytiala, Finland, Boreal Environment Research, 10(5), 323–336, 2005.

Deng, Z. Z., Zhao, C. S., Ma, N., Liu, P. F., Ran, L., Xu, W. Y., Chen, J., Liang, Z., Liang, S., Huang, M. Y., Ma, X. C., Zhang, Q., Quan, J. N., Yan, P., Henning, S., Mildenberger, K., Sommerhage, E., Schäfer, M., Stratmann, F. and Wiedensohler, A.: Size-resolved and bulk activation properties of aerosols in the North China Plain, Atmos. Chem. Phys., 11(8), 3835–3846, doi:10.5194/acp-11-3835-2011, 2011.

Deng, Z. Z., Zhao, C. S., Ma, N., Ran, L., Zhou, G. Q., Lu, D. R. and Zhou, X. J.: An examination of parameterizations for the CCN number concentration based on in situ measurements of aerosol activation properties in the North China Plain, Atmos. Chem. Phys., 13(13), 6227–6237, doi:10.5194/acp-13-6227-2013, 2013.

Ditas, F., Shaw, R. A., Siebert, H., Simmel, M., Wehner, B. and Wiedensohler, A.: Aerosols-cloud microphysics-thermodynamics-turbulence: evaluating supersaturation in a marine stratocumulus cloud, Atmos. Chem. Phys., 12(5), 2459–2468, doi:10.5194/acp-12-2459-2012, 2012.

Duan, J., Wang, Y., Xie, X., Li, M., Tao, J., Wu, Y., Cheng, T., Zhang, R., Liu, Y., Li, X., He, Q., Gao, W. and Wang, J.: Influence of pollutants on activity of aerosol cloud condensation nuclei (CCN) during pollution and post-rain periods in Guangzhou, southern China, Science of the Total Environment, 642, 1008–1019, doi:10.1016/j.scitotenv.2018.06.053, 2018.

Fan, J., Wang, Y., Rosenfeld, D. and Liu, X.: Review of Aerosol–Cloud Interactions: Mechanisms, Significance, and Challenges, Journal of the Atmospheric Sciences, 73(11), 4221–4252, doi:10.1175/JAS-D-16-0037.1, 2016.

Farmer, D. K., Cappa, C. D. and Kreidenweis, S. M.: Atmospheric Processes and Their Controlling Influence on Cloud Condensation Nuclei Activity, Chemical Reviews, 115(10), 4199–4217, doi:10.1021/cr5006292, 2015.

https://doi.org/10.5194/acp-2020-939
Preprint. Discussion started: 12 October 2020


Atmospheric Chemistry and Physics Discussions

570 Gryspeerdt, E. and Stier, P.: Regime-based analysis of aerosol-cloud interactions, Geophysical
571 Research Letters, 39(21), doi:10.1029/2012GL053221, 2012.

572 Gysel, M., Crosier, J., Topping, D. O., Whitehead, J. D., Bower, K. N., Cubison, M. J., Williams, P.
573 I., Flynn, M. J., McFiggans, G. B. and Coe, H.: Closure study between chemical composition and
574 hygroscopic growth of aerosol particles during TORCH2, Atmos. Chem. Phys., 7(24), 6131–6144,
575 doi:10.5194/acp-7-6131-2007, 2007.

576 Gysel, M., McFiggans, G. B. and Coe, H.: Inversion of tandem differential mobility analyser (TDMA)
577 measurements, Journal of Aerosol Science, 40(2), 134–151, doi:10.1016/j.jaerosci.2008.07.013, 2009.

578 Hagen, D. E. and Alofs, D. J.: Linear Inversion Method to Obtain Aerosol Size Distributions from
579 Measurements with a Differential Mobility Analyzer, Aerosol Science and Technology, 2(4), 465–
580 475, doi:10.1080/02786828308958650, 1983.

581 Hammer, E., Bukowiecki, N., Gysel, M., Jurányi, Z., Hoyle, C. R., Vogt, R., Baltensperger, U. and
582 Weingartner, E.: Investigation of the effective peak supersaturation for liquid-phase clouds at the high-
583 alpine site Jungfraujoch, Switzerland (3580 m a.s.l.), Atmos. Chem. Phys., 14(2), 1123–1139,
584 doi:10.5194/acp-14-1123-2014, 2014a.

585 Hammer, E., Gysel, M., Roberts, G. C., Elias, T., Hofer, J., Hoyle, C. R., Bukowiecki, N., Dupont, J.-
586 C., Burnet, F., Baltensperger, U. and Weingartner, E.: Size-dependent particle activation properties in
587 fog during the ParisFog 2012/13 field campaign, Atmos. Chem. Phys., 14(19), 10517–10533,
588 doi:10.5194/acp-14-10517-2014, 2014b.

589 Hong, J., Xu, H., Tan, H., Yin, C. and Kerminen, V. M.: Mixing state and particle hygroscopicity of
590 organic-dominated aerosols over the Pearl River Delta region in China, Atmos. Chem. Phys., 18(19),
591 14079–14094, 2018.

592 Hu, W., Hu, M., Hu, W., Jimenez, J. L., Yuan, B., Chen, W., Wang, M., Wu, Y., Chen, C., Wang, Z.,
593 Peng, J., Zeng, L. and Shao, M.: Chemical composition, sources, and aging process of submicron
594 aerosols in Beijing: Contrast between summer and winter, Journal of Geophysical Research:
595 Atmospheres, 121(4), 1955–1977, doi:10.1002/2015JD024020, 2016.

596 Hu, W., Campuzano-Jost, P., Day, D. A., Croteau, P., Canagaratna, M. R., Jayne, J. T., Worsnop, D.
597 R. and Jimenez, J. L.: Evaluation of the new capture vapourizer for aerosol mass spectrometers (AMS)
598 through laboratory studies of inorganic species, Atmos. Meas. Tech., 10(8), 2897–2921,
599 doi:10.5194/amt-10-2897-2017, 2017a.

https://doi.org/10.5194/acp-2020-939
Preprint. Discussion started: 12 October 2020


Atmospheric Chemistry and Physics Discussions

600 Hu, W., Hu, M., Hu, W.-W., Zheng, J., Chen, C., Wu, Y. and Guo, S.: Seasonal variations in high
601 time-resolved chemical compositions, sources, and evolution of atmospheric submicron aerosols in
602 the megacity Beijing, Atmos. Chem. Phys., 17(16), 9979–10000, doi:10.5194/acp-17-9979-2017,
603 2017b.

604 Huang, R.-J., Zhang, Y., Bozzetti, C., Ho, K.-F., Cao, J.-J., Han, Y., Daellenbach, K. R., Slowik, J. G.,
605 Platt, S. M., Canonaco, F., Zotter, P., Wolf, R., Pieber, S. M., Bruns, E. A., Crippa, M., Ciarelli, G.,
606 Piazzalunga, A., Schwikowski, M., Abbaszade, G., Schnelle-Kreis, J., Zimmermann, R., An, Z., Szidat,
607 S., Baltensperger, U., Haddad, I. E. and Prévôt, A. S. H.: High secondary aerosol contribution to
608 particulate pollution during haze events in China, Nature, 514(7521), 218–222,
609 doi:10.1038/nature13774, 2014.

610 Jia, H., Ma, X., Yu, F., Liu, Y. and Yin, Y.: Distinct Impacts of Increased Aerosols on Cloud Droplet
611 Number Concentration of Stratus/Stratocumulus and Cumulus, Geophysical Research Letters, n/a(n/a),
612 doi:10.1029/2019GL085081, 2019.

613 Kerminen, V.-M., Paramonov, M., Anttila, T., Riipinen, I., Fountoukis, C., Korhonen, H., Asmi, E.,
614 Laakso, L., Lihavainen, H., Swietlicki, E., Svenningsson, B., Asmi, A., Pandis, S. N., Kulmala, M.
615 and Petaja, T.: Cloud condensation nuclei production associated with atmospheric nucleation: a
616 synthesis based on existing literature and new results, Atmospheric Chemistry and Physics, 12(24),
617 12037–12059, doi:10.5194/acp-12-12037-2012, 2012.

618 Köhler, H.: The nucleus in and the growth of hygroscopic droplets, Transactions of the Faraday Society,
619 32, 1152–1161, 1936.

620 Krüger, M. L., Mertes, S., Klimach, T., Cheng, Y. F., Su, H., Schneider, J., Andreae, M. O., Pöschl,
621 U. and Rose, D.: Assessment of cloud supersaturation by size-resolved aerosol particle and cloud
622 condensation nuclei (CCN) measurements, Atmos. Meas. Tech., 7(8), 2615–2629, doi:10.5194/amt-
623 7-2615-2014, 2014.

624 Kuang, Y., He, Y., Xu, W., Zhao, P., Cheng, Y., Zhao, G., Tao, J., Ma, N., Su, H., Zhang, Y., Sun, J.,
625 Cheng, P., Yang, W., Zhang, S., Wu, C., Sun, Y. and Zhao, C.: Distinct diurnal variation in organic
626 aerosol hygroscopicity and its relationship with oxygenated organic aerosol, Atmos. Chem. Phys.,
627 20(2), 865–880, doi:10.5194/acp-20-865-2020, 2020a.

628 Kuang, Y., He, Y., Xu, W., Yuan, B., Zhang, G., Ma, Z., Wu, C., Wang, C., Wang, S., Zhang, S., Tao,
629 J., Ma, N., Su, H., Cheng, Y., Shao, M. and Sun, Y.: Photochemical Aqueous-Phase Reactions Induce
630 Rapid Daytime Formation of Oxygenated Organic Aerosol on the North China Plain, Environmental
631 Science & Technology, 54(7), 3849–3860, doi:10.1021/acs.est.9b06836, 2020b.

https://doi.org/10.5194/acp-2020-939
Preprint. Discussion started: 12 October 2020


Atmospheric Chemistry and Physics Discussions

632 Kulmala, M., Riipinen, I., Sipila, M., Manninen, H. E., Petaja, T., Junninen, H., Dal Maso, M., Mordas,
633 G., Mirme, A., Vana, M., Hirsikko, A., Laakso, L., Harrison, R. M., Hanson, I., Leung, C., Lehtinen,
634 K. E. J. and Kerminen, V.-M.: Toward direct measurement of atmospheric nucleation, Science,
635 318(5847), 89–92, doi:10.1126/science.1144124, 2007.

636 Liu, H. J., Zhao, C. S., Nekat, B., Ma, N., Wiedensohler, A., van Pinxteren, D., Spindler, G., Müller,
637 K. and Herrmann, H.: Aerosol hygroscopicity derived from size-segregated chemical composition and
638 its parameterization in the North China Plain, Atmos. Chem. Phys., 14(5), 2525–2539,
639 doi:10.5194/acp-14-2525-2014, 2014.

640 Liu, Z., Wang, Y., Gu, D., Zhao, C., Huey, L. G., Stickel, R., Liao, J., Shao, M., Zhu, T., Zeng, L.,
641 Liu, S.-C., Chang, C.-C., Amoroso, A. and Costabile, F.: Evidence of Reactive Aromatics As a Major
642 Source of Peroxy Acetyl Nitrate over China, Environ. Sci. Technol., 44(18), 7017–7022,
643 doi:10.1021/es1007966, 2010.

644 Ma, N., Zhao, C., Tao, J., Wu, Z., Kecorius, S., Wang, Z., Größ, J., Liu, H., Bian, Y., Kuang, Y., Teich,
645 M., Spindler, G., Müller, K., van Pinxteren, D., Herrmann, H., Hu, M. and Wiedensohler, A.: Variation
646 of CCN activity during new particle formation events in the North China Plain, Atmos. Chem. Phys.,
647 16(13), 8593–8607, doi:10.5194/acp-16-8593-2016, 2016.

648 Mei, F., Hayes, P. L., Ortega, A., Taylor, J. W., Allan, J. D., Gilman, J., Kuster, W., de Gouw, J.,
649 Jimenez, J. L. and Wang, J.: Droplet activation properties of organic aerosols observed at an urban site
650 during CalNex-LA, Journal of Geophysical Research-Atmospheres, 118(7), 2903–2917,
651 doi:10.1002/jgrd.50285, 2013.

652 Petters, M. D. and Kreidenweis, S. M.: A single parameter representation of hygroscopic growth and
653 cloud condensation nucleus activity, Atmos. Chem. Phys., 7(8), 1961–1971, 2007.

654 Reutter, P., Su, H., Trentmann, J., Simmel, M., Rose, D., Gunthe, S. S., Wernli, H., Andreae, M. O.
655 and Pöschl, U.: Aerosol- and updraft-limited regimes of cloud droplet formation: influence of particle
656 number, size and hygroscopicity on the activation of cloud condensation nuclei (CCN), Atmos. Chem.
657 Phys., 9(18), 7067–7080, doi:10.5194/acp-9-7067-2009, 2009.

658 Roberts, G. C. and Nenes, A.: A continuous-flow streamwise thermal-gradient CCN chamber for
659 atmospheric measurements, Aerosol science and technology, 39(3), 206–221, 2005.

660 Rose, D., Gunthe, S. S., Mikhailov, E., Frank, G. P., Dusek, U., Andreae, M. O. and Pöschl, U.:
661 Calibration and measurement uncertainties of a continuous-flow cloud condensation nuclei counter

https://doi.org/10.5194/acp-2020-939
Preprint. Discussion started: 12 October 2020


Atmospheric Chemistry and Physics Discussions

(DMT-CCNC): CCN activation of ammonium sulfate and sodium chloride aerosol particles in theory and experiment, Atmos. Chem. Phys., 8(5), 1153–1179, 2008.

Rose, D., Nowak, A., Achtert, P., Wiedensohler, A., Hu, M., Shao, M., Zhang, Y., Andreae, M. O. and Poschl, U.: Cloud condensation nuclei in polluted air and biomass burning smoke near the mega-city Guangzhou, China - Part 1: Size-resolved measurements and implications for the modeling of aerosol particle hygroscopicity and CCN activity, Atmos. Chem. Phys., 10(7), 3365–3383, 2010.

Shen, C., Zhao, C., Ma, N., Tao, J., Zhao, G., Yu, Y. and Kuang, Y.: Method to Estimate Water Vapor Supersaturation in the Ambient Activation Process Using Aerosol and Droplet Measurement Data, Journal of Geophysical Research: Atmospheres, 123(18), 10,606-10,619, doi:10.1029/2018JD028315, 2018.

Sun, Y., He, Y., Kuang, Y., Xu, W., Song, S., Ma, N., Tao, J., Cheng, P., Wu, C., Su, H., Cheng, Y., Xie, C., Chen, C., Lei, L., Qiu, Y., Fu, P., Croteau, P. and Worsnop, D. R.: Chemical Differences Between PM1 and PM2.5 in Highly Polluted Environment and Implications in Air Pollution Studies, Geophysical Research Letters, 47(5), e2019GL086288, doi:10.1029/2019GL086288, 2020.

Tan, H., Xu, H., Wan, Q., Li, F., Deng, X., Chan, P. W., Xia, D. and Yin, Y.: Design and Application of an Unattended Multifunctional H-TDMA System, Journal of Atmospheric and Oceanic Technology, 30(6), 1136–1148, doi:10.1175/JTECH-D-12-00129.1, 2013.

Tao, J., Kuang, Y., Ma, N., Zheng, Y., Wiedensohler, A. and Zhao, C.: An improved parameterization scheme for size-resolved particle activation ratio and its application on comparison study of particle hygroscopicity measurements between HTDMA and DMA-CCNC, Atmospheric Environment, 226, 117403, doi:10.1016/j.atmosenv.2020.117403, 2020.

Thalman, R., de Sa, S. S., Palm, B. B., Barbosa, H. M. J., Poehlker, M. L., Alexander, M. L., Brito, J., Carbone, S., Castillo, P., Day, D. A., Kuang, C., Manzi, A., Ng, N. L., Sedlacek, A. J., Souza, R., Springston, S., Watson, T., Poehlker, C., Poeschl, U., Andreae, M. O., Artaxo, P., Jimenez, J. L., Martin, S. T. and Wang, J.: CCN activity and organic hygroscopicity of aerosols downwind of an urban region in central Amazonia: seasonal and diel variations and impact of anthropogenic emissions, Atmospheric Chemistry and Physics, 17(19), 11779–11801, doi:10.5194/acp-17-11779-2017, 2017.

Wang, Y., Chen, J., Wang, Q., Qin, Q., Ye, J., Han, Y., Li, L., Zhen, W., Zhi, Q., Zhang, Y. and Cao, J.: Increased secondary aerosol contribution and possible processing on polluted winter days in China, Environment International, 127, 78–84, doi:10.1016/j.envint.2019.03.021, 2019.

https://doi.org/10.5194/acp-2020-939
Preprint. Discussion started: 12 October 2020

692 Wiedensohler, A., Cheng, Y. F., Nowak, A., Wehner, B., Achtert, P., Berghof, M., Birmili, W., Wu,
693 Z. J., Hu, M., Zhu, T., Takegawa, N., Kita, K., Kondo, Y., Lou, S. R., Hofzumahaus, A., Holland, F.,
694 Wahner, A., Gunthe, S. S., Rose, D., Su, H. and Poeschl, U.: Rapid aerosol particle growth and increase
695 of cloud condensation nucleus activity by secondary aerosol formation and condensation: A case study
696 for regional air pollution in northeastern China, Journal of Geophysical Research-Atmospheres, 114,
697 D00G08, doi:10.1029/2008JD010884, 2009.

698 Williams, B. J., Goldstein, A. H., Kreisberg, N. M., Hering, S. V., Worsnop, D. R., Ulbrich, I. M.,
699 Docherty, K. S. and Jimenez, J. L.: Major components of atmospheric organic aerosol in southern
700 California as determined by hourly measurements of source marker compounds, Atmos. Chem. Phys.,
701 10(23), 11577–11603, doi:10.5194/acp-10-11577-2010, 2010.

702 Wu, Z. J., Poulain, L., Birmili, W., Groess, J., Niedermeier, N., Wang, Z. B., Herrmann, H. and
703 Wiedensohler, A.: Some insights into the condensing vapors driving new particle growth to CCN sizes
704 on the basis of hygroscopicity measurements, Atmospheric Chemistry and Physics, 15(22), 13071–
705 13083, doi:10.5194/acp-15-13071-2015, 2015.

706 Wu, Z. J., Zheng, J., Shang, D. J., Du, Z. F., Wu, Y. S., Zeng, L. M., Wiedensohler, A. and Hu, M.:
707 Particle hygroscopicity and its link to chemical composition in the urban atmosphere of Beijing, China,
708 during summertime, Atmos. Chem. Phys., 16(2), 1123–1138, doi:10.5194/acp-16-1123-2016, 2016.

709 Xu, W., Han, T., Du, W., Wang, Q., Chen, C., Zhao, J., Zhang, Y., Li, J., Fu, P., Wang, Z., Worsnop,
710 D. R. and Sun, Y.: Effects of Aqueous-Phase and Photochemical Processing on Secondary Organic
711 Aerosol Formation and Evolution in Beijing, China, Environ. Sci. Technol., 51(2), 762–770,
712 doi:10.1021/acs.est.6b04498, 2017a.

713 Xu, W., Croteau, P., Williams, L., Canagaratna, M., Onasch, T., Cross, E., Zhang, X., Robinson, W.,
714 Worsnop, D. and Jayne, J.: Laboratory characterization of an aerosol chemical speciation monitor with
715 PM2.5 measurement capability, Aerosol Science and Technology, 51(1), 69–83,
716 doi:10.1080/02786826.2016.1241859, 2017b.

717 Xu, W., Sun, Y., Wang, Q., Zhao, J., Wang, J., Ge, X., Xie, C., Zhou, W., Du, W., Li, J., Fu, P., Wang,
718 Z., Worsnop, D. R. and Coe, H.: Changes in Aerosol Chemistry From 2014 to 2016 in Winter in
719 Beijing: Insights From High-Resolution Aerosol Mass Spectrometry, Journal of Geophysical Research:
720 Atmospheres, 124(2), 1132–1147, doi:10.1029/2018JD029245, 2019.

721 Xu, W. Q., Sun, Y. L., Chen, C., Du, W., Han, T. T., Wang, Q. Q., Fu, P. Q., Wang, Z. F., Zhao, X. J.,
722 Zhou, L. B., Ji, D. S., Wang, P. C. and Worsnop, D. R.: Aerosol composition, oxidation properties,

https://doi.org/10.5194/acp-2020-939
Preprint. Discussion started: 12 October 2020


Atmospheric Chemistry and Physics Discussions

723 and sources in Beijing: results from the 2014 Asia-Pacific Economic Cooperation summit study,
724 Atmos. Chem. Phys., 15(23), 13681–13698, doi:10.5194/acp-15-13681-2015, 2015.

725 Yue, D., Zhong, L., Zhang, T., Shen, J., Yuan, L., Ye, S., Zhou, Y. and Zeng, L.: Particle Growth and
726 Variation of Cloud Condensation Nucleus Activity on Polluted Days with New Particle Formation: A
727 Case Study for Regional Air Pollution in the PRD Region, China, Aerosol and Air Quality Research,
728 16(2), 323–335, doi:10.4209/aaqr.2015.06.0381, 2016.

729 Zhang, F., Ren, J., Fan, T., Chen, L., Xu, W., Sun, Y., Zhang, R., Liu, J., Jiang, S., Jin, X., Wu, H., Li,
730 S., Cribb, M. C. and Li, Z.: Significantly enhanced aerosol CCN activity and number concentrations
731 by nucleation-initiated haze events: a case study in urban Beijing, Journal of Geophysical Research:
732 Atmospheres, n/a(n/a), doi:10.1029/2019JD031457, 2019.

733 Zhang, Q., Jimenez, J. L., Canagaratna, M. R., Ulbrich, I. M., Ng, N. L., Worsnop, D. R. and Sun, Y.:
734 Understanding atmospheric organic aerosols via factor analysis of aerosol mass spectrometry: a review,
735 Analytical and Bioanalytical Chemistry, 401(10), 3045–3067, doi:10.1007/s00216-011-5355-y, 2011.

736 Zhang, R., Khalizov, A., Wang, L., Hu, M. and Xu, W.: Nucleation and Growth of Nanoparticles in
737 the Atmosphere, Chemical Reviews, 112(3), 1957–2011, doi:10.1021/cr2001756, 2012.

738 Chang, R. Y.-W., Slowik, J. G., Shantz, N. C., Vlasenko, A., Liggio, J., Sjostedt, S. J., Leaitch, W. R.
739 and Abbatt, J. P. D.: The hygroscopicity parameter (κ) of ambient organic aerosol at a field site subject
740 to biogenic and anthropogenic influences: relationship to degree of aerosol oxidation, Atmos. Chem.
741 Phys., 10(11), 5047–5064, doi:10.5194/acp-10-5047-2010, 2010.

742 Cheng, Y. F., Su, H., Rose, D., Gunthe, S. S., Berghof, M., Wehner, B., Achtert, P., Nowak, A.,
743 Takegawa, N., Kondo, Y., Shiraiwa, M., Gong, Y. G., Shao, M., Hu, M., Zhu, T., Zhang, Y. H.,
744 Carmichael, G. R., Wiedensohler, A., Andreae, M. O. and Pöschl, U.: Size-resolved measurement of
745 the mixing state of soot in the megacity Beijing, China: diurnal cycle, aging and parameterization,
746 Atmos. Chem. Phys., 12(10), 4477–4491, doi:10.5194/acp-12-4477-2012, 2012.

747 Dusek, U., Frank, G., Hildebrandt, L., Curtius, J., Schneider, J., Walter, S., Chand, D., Drewnick, F.,
748 Hings, S. and Jung, D.: Size matters more than chemistry for cloud-nucleating ability of aerosol
749 particles, Science, 312(5778), 1375–1378, 2006.

750 Gordon, H., Sengupta, K., Rap, A., Duplissy, J., Frege, C., Williamson, C., Heinritzi, M., Simon, M.,
751 Yan, C., Almeida, J., Trostl, J., Nieminen, T., Ortega, I. K., Wagner, R., Dunne, E. M., Adamov, A.,
752 Amorim, A., Bernhammer, A.-K., Bianchi, F., Breitenlechner, M., Brilke, S., Chen, X., Craven, J. S.,
753 Dias, A., Ehrhart, S., Fischer, L., Flagan, R. C., Franchin, A., Fuchs, C., Guida, R., Hakala, J., Hoyle,

https://doi.org/10.5194/acp-2020-939
Preprint. Discussion started: 12 October 2020

C. R., Jokinen, T., Junninen, H., Kangasluoma, J., Kim, J., Kirkby, J., Krapf, M., Kuerten, A., Laaksonen, A., Lehtipalo, K., Makhmutov, V., Mathot, S., Molteni, U., Monks, S. A., Onnela, A., Perakyla, O., Piel, F., Petaja, T., Praplan, A. P., Pringle, K. J., Richards, N. A. D., Rissanen, M. P., Rondo, L., Sarnela, N., Schobesberger, S., Scott, C. E., Seinfeldo, J. H., Sharma, S., Sipila, M., Steiner, G., Stozhkov, Y., Stratmann, F., Tome, A., Virtanen, A., Vogel, A. L., Wagner, A. C., Wagner, P. E., Weingartner, E., Wimmer, D., Winkler, P. M., Ye, P., Zhang, X., Hansel, A., Dommen, J., Donahue, N. M., Worsnop, D. R., Baltensperger, U., Kulmala, M., Curtius, J. and Carslaw, K. S.: Reduced anthropogenic aerosol radiative forcing caused by biogenic new particle formation, Proceedings of the National Academy of Sciences of the United States of America, 113(43), 12053–12058, doi:10.1073/pnas.1602360113, 2016.

Kawana, K., Nakayama, T. and Mochida, M.: Hygroscopicity and CCN activity of atmospheric aerosol particles and their relation to organics: Characteristics of urban aerosols in Nagoya, Japan, Journal of Geophysical Research: Atmospheres, 121(8), 4100–4121, doi:10.1002/2015jd023213, 2016.

Rose, D., Gunthe, S. S., Su, H., Garland, R. M., Yang, H., Berghof, M., Cheng, Y. F., Wehner, B., Achtert, P., Nowak, A., Wiedensohler, A., Takegawa, N., Kondo, Y., Hu, M., Zhang, Y., Andreae, M. O. and Poschl, U.: Cloud condensation nuclei in polluted air and biomass burning smoke near the mega-city Guangzhou, China -Part 2: Size-resolved aerosol chemical composition, diurnal cycles, and externally mixed weakly CCN-active soot particles, Atmos. Chem. Phys., 11(6), 2817–2836, doi:10.5194/acp-11-2817-2011, 2011.

Su, H., Rose, D., Cheng, Y. F., Gunthe, S. S., Massling, A., Stock, M., Wiedensohler, A., Andreae, M. O. and Poschl, U.: Hygroscopicity distribution concept for measurement data analysis and modeling of aerosol particle mixing state with regard to hygroscopic growth and CCN activation, Atmos. Chem. Phys., 10(15), 7489–7503, doi:10.5194/acp-10-7489-2010, 2010.

Yu, F., Luo, G., Nair, A. A., Schwab, J. J., Sherman, J. P. and Zhang, Y.: Wintertime new particle formation and its contribution to cloud condensation nuclei in the Northeastern United States, Atmos. Chem. Phys., 20(4), 2591–2601, doi:10.5194/acp-20-2591-2020, 2020.

Guo Li, Hang Su, Nan Ma, Jiangchuan Tao, Ye Kuang, Qiaoqiao Wang, Juan Hong, Yuxuan Zhang, Uwe Kuhn, Shaobin Zhang, Xihao Pan, Nan Lu, Min Tang, Guangjie Zheng, Yang Gao, Peng Cheng,e Wanyun Xu, Chunsheng Zhao, Bin Yuan, Min Shao, Aijun Ding, Qiang Zhang, Pingqing Fu, Yele Sun, Ulrich Pöschl and Yafang Cheng: Multiphase chemistry experiment in Fogs and Aerosols in the North China Plain (McFAN): integrated analysis and intensive winter campaign 2018, Faraday Discussions, submitted.

https://doi.org/10.5194/acp-2020-939
Preprint. Discussion started: 12 October 2020

Atmospheric Chemistry and Physics Discussions

786 **Figures:**

787

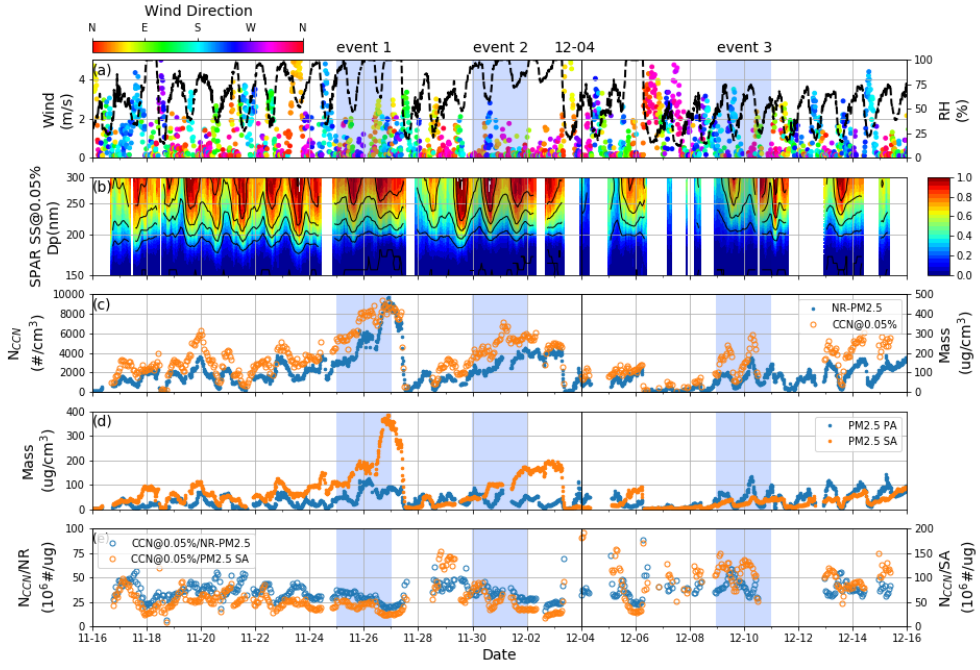

788

789 Fig 1. Overview of the measurements during the campaign: (a) dots represent wind speed with color
790 indicating wind direction, and black lines represent RH; (b) SPAR under SS of 0.05%; (c) blue dots
791 represent N_{CCN} under SS of 0.05% and yellow dots represent mass concentration of NR-$PM_{2.5}$; (d)
792 blue and yellow dots represent mass concentration of $PM_{2.5}$ PA and $PM_{2.5}$ SA respectively; (e) blue
793 and yellow dots represent ratio between N_{CCN} and mass concentration of NR-$PM_{2.5}$ and $PM_{2.5}$ SA,
794 respectively. There were three events with significant enhancements of N_{CCN} during the blue shaded
795 periods.

https://doi.org/10.5194/acp-2020-939
Preprint. Discussion started: 12 October 2020

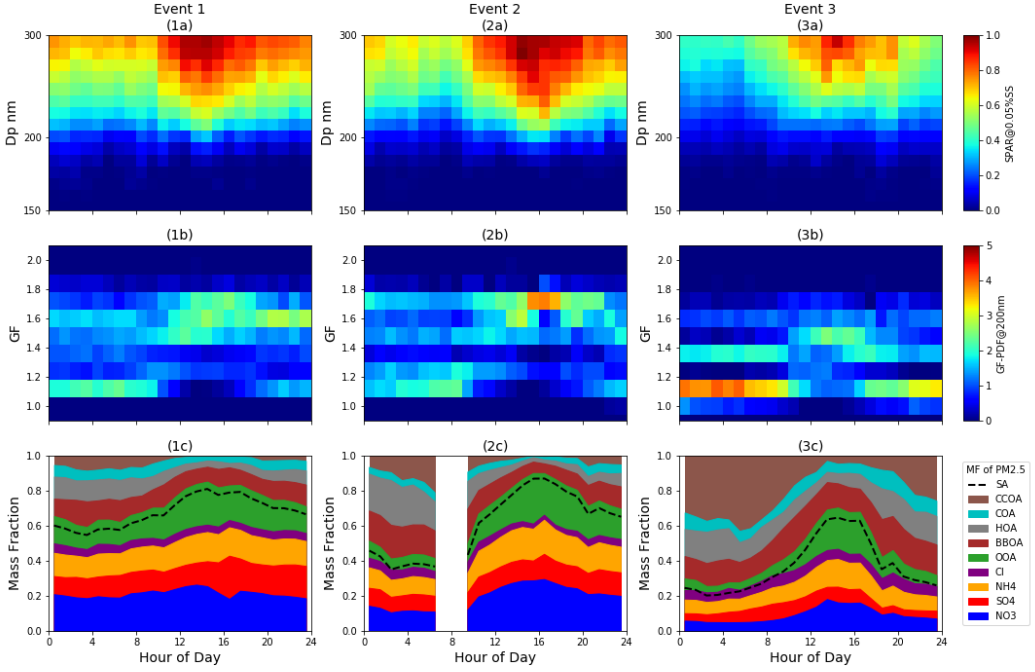

Fig 2. Diurnal variation of (a) SPAR at SS of 0.05%, (b) GF-PDF at 200nm and (c) mass fraction of different $PM_{2.5}$ chemical species during the three events.

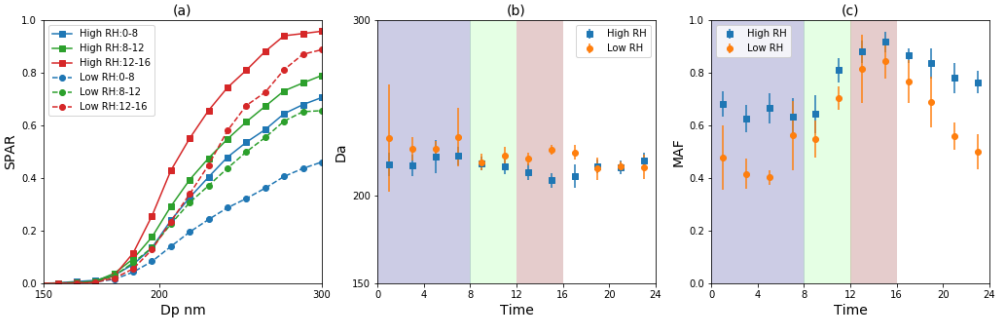

Fig 3. (a) The averages of SPAR curves at SS of 0.05% in three different time periods (blue: 0:00-8:00; green: 8:00-12:00; red: 12:00-16:00) during high (squares with solid line) and low (dots with dashed line) RH events. Diurnal variation of (b) Da and (c) MAF under high (blue) and low (yellow) RH conditions. The blue, green and red shades correspond to with the three periods in (a).

https://doi.org/10.5194/acp-2020-939
Preprint. Discussion started: 12 October 2020

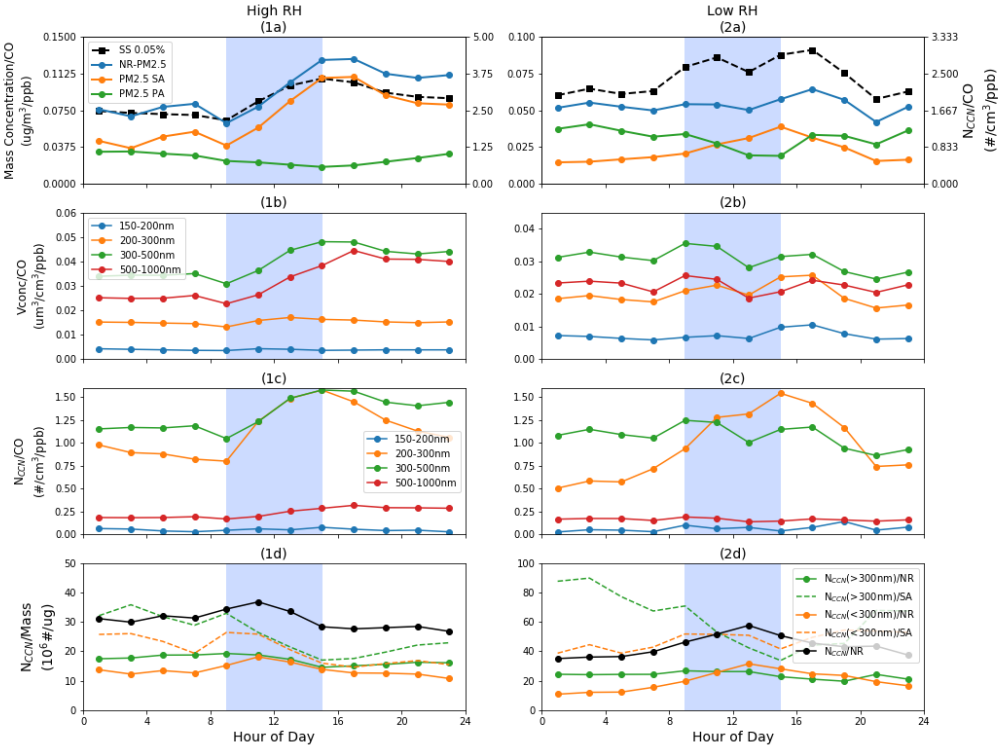

806

807 Fig 4. During different RH events, the average diurnal variation of (a) the ratios between particle
808 mass concentration (dots with solid lines; blue: NR-$PM_{2.5}$; yellow: $PM_{2.5}$ SA; green: $PM_{2.5}$ PA) and
809 CO concentration, and the ratio between N_{CCN} at SS of 0.05% and CO concentration (squares with
810 solid line); (b) the ratios between particle volume concentration (Vconc) of different particle size
811 range (indicated by colors) and CO concentration; (c) the ratios between N_{CCN} of different particle
812 size range at SS of 0.05% (indicated by colors) and CO concentration; (d) the ratios between N_{CCN} at
813 SS of 0.05% (black: bulk N_{CCN}; yellow: N_{CCN} with particle size larger than 300nm; blue: N_{CCN} with
814 particle size smaller than 300nm) and mass concentration of NR-$PM_{2.5}$ SA and the ratios between
815 N_{CCN} and mass concentration of NR-$PM_{2.5}$ (dashed lines).

816

https://doi.org/10.5194/acp-2020-939
Preprint. Discussion started: 12 October 2020

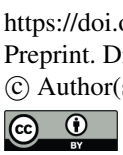

Atmospheric Chemistry and Physics Discussions

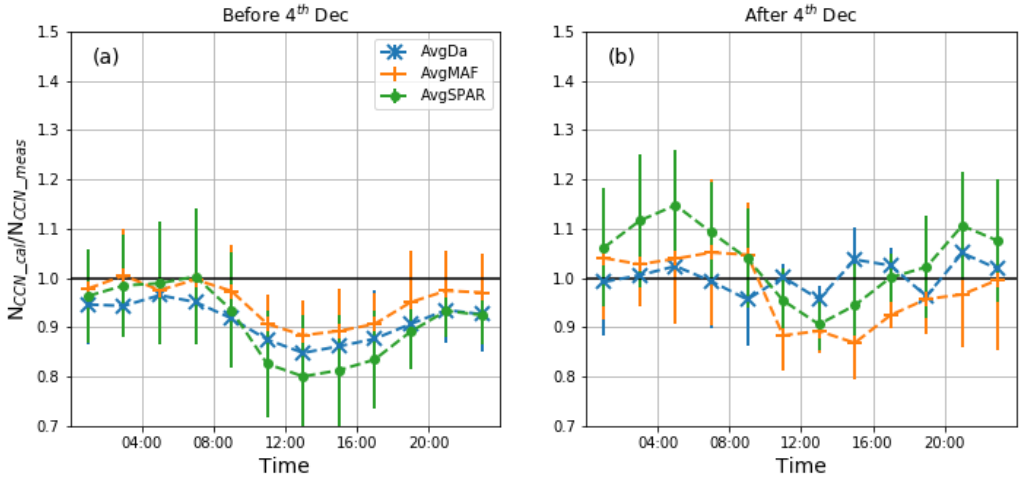

817

818 Fig 5. The ratio between calculated N_{CCN} and measured N_{CCN} under (a) before 12-04 and (b) after
819 12-04. Bars represent one standard deviation and colors represent different calculation of SPAR
820 curves: green represent average SPAR during the campaign (AvgSPAR), yellow represent SPAR
821 calculated with average Da and real-time MAF (AvgDa) and blue represent SPAR calculated with
822 average MAF and real-time Da (AvgMAF).

823

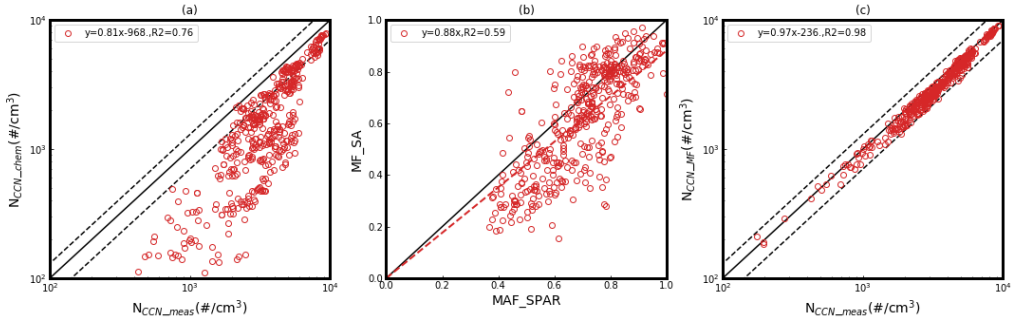

824

825 Fig 6. (a) the comparison between calculated N_{CCN} based on kappa derived from bulk particle chemical
826 compositions (N_{CCN_chem}) and measured N_{CCN} at SS of 0.05%. (b) The correlation between MAF and
827 mass fraction of secondary aerosol (MF_SA). (c) the comparison between calculated N_{CCN} based on
828 SPAR derived from real-time MF_SA and average Da (N_{CCN_MF}) and measured N_{CCN}. The black
829 dashed lines represent the relative deviation of 30%.

830

https://doi.org/10.5194/acp-2020-939
Preprint. Discussion started: 12 October 2020

Atmospheric Chemistry and Physics Discussions

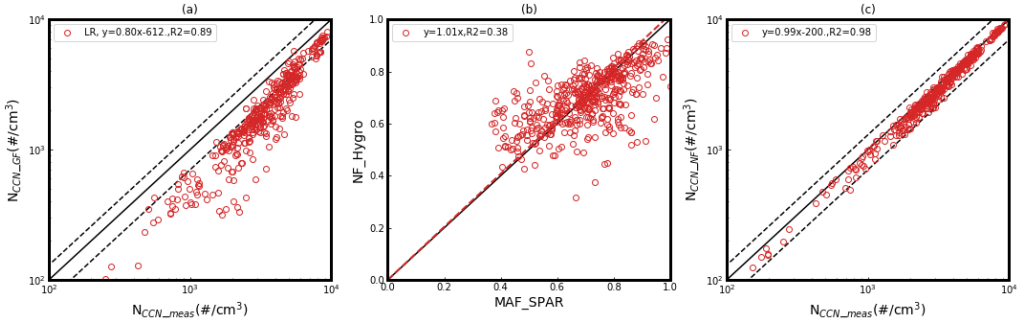

831

832 Fig 7. (a) The comparison between calculated N_{CCN} based on kappa derived from bulk GF at 200 nm
833 (N_{CCN_GF}) and measured N_{CCN} at SS of 0.05%. (b) The correlation between MAF and number fraction
834 of hygroscopic particles (NF_hygro, GF>1.2). (c) The comparison between calculated N_{CCN} based on
835 SPAR derived from real-time NF_hygro and average Da (N_{CCN_NF}) and measured N_{CCN}. The black
836 dashed lines represent the relative deviation of 30%.